Design of a Closed-Loop Wireless Power Transfer System for an Implantable Drug Delivery Device

Design of a Closed-Loop Wireless Power Transfer System for an Implantable Drug Delivery Device

Fabiana Del Bono, *Graduate Student Member, IEEE*, Andrea Bontempi, *Graduate Student Member, IEEE*, Andrea Dentis, Nicola Di Trani, Danilo Demarchi, *Senior Member, IEEE*, Alessandro Grattoni, and Paolo Motto Ros, *Member, IEEE*

***Abstract*—Active implantable medical devices (AIMDs) have seen a significant increase in popularity in recent years due to their ability to provide continuous therapy unobtrusively. One of the key challenges in developing next-generation AIMDs is the design of a safe and reliable wireless power transfer (WPT) system. Standard commercial WPT components are not optimized to deliver small amounts of power or to work with other than small air gaps. We developed a near-field resonant inductive coupling (NRIC) WPT system with closed-loop real-time control, based on the commercial off-the-shelf (COTS) components and leveraging the already integrated wireless communication system. The system was used to recharge a secondary battery and power supply the nanochannel delivery system (nDS). We tested the system's robustness by varying the coil spacing to a maximum of 20 mm, and by misaligning the coils laterally and angularly up to 8 mm and 12°, respectively. We performed these tests by simulating battery charging from 2.8 to 4.1 V and we tested four coils, from 6 to 19 mm in diameter, to evaluate the best tradeoff between effectiveness and miniaturization. Finally, we recharged the selected battery for two distances, 2.5 and 6.5 mm. The results show that the 17- and 19-mm coils have the highest peak efficiencies of 31.3% and 32.3% (26% and 26.3% on average), respectively, and provide a complete and reliable battery recharge in less than 5 h while keeping the receiver coil temperature within 2 °C.**

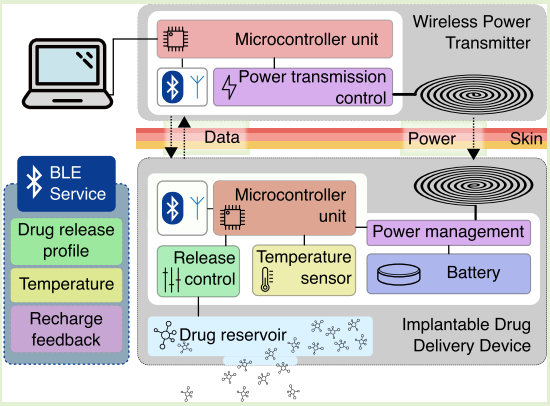

***Index Terms*— Active implantable medical devices (AIMDs), nanochannel delivery system (nDS), near-field resonant inductive coupling (NRIC), wireless power transfer (WPT).**

I. Introduction

ACTIVE implantable medical devices (AIMDs) are surgically implanted within the human body to provide continuous or intermittent therapy. AIMDs treat various medical conditions, including chronic diseases that develop gradually and can be managed but are not always completely cured. Some examples of chronic pathologies include diabetes, heart disease, asthma, and kidney disease. These can cause long-term complications and increase the risk of premature death. Prevention and early treatment are essential in effectively managing chronic diseases. AIMDs can help improve patient's quality of life and prevent long-term complications. However, specific challenges must be overcome to fully exploit these systems' potential. One of the most critical considerations in the design of implantable systems is represented by the volume constraints [1], [2]. This is because device discreetness and patient acceptability are of utmost importance in this field, much more than for wearable internet of things (IoT) devices [3], [4]. The next generation of advanced AIMDs aims to address these challenges by minimizing the overall size and power consumption, while

Manuscript received 1 February 2023; revised 7 April 2023; accepted 14 April 2023. Date of publication 3 May 2023; date of current version 14 March 2024. The associate editor coordinating the review of this article and approving it for publication was Dr. Rolland Vida. *(Corresponding author: Fabiana Del Bono.)*

Fabiana Del Bono, Andrea Bontempi, Andrea Dentis, Danilo Demarchi, and Paolo Motto Ros are with the Department of Electronics and Telecommunications (DET), Politecnico di Torino, 10129 Turin, Italy (e-mail: fabiana.delbono@polito.it; andrea.bontempi@polito.it; andrea.dentis@studenti.polito.it; danilo.demarchi@polito.it; paolo.mottoros@polito.it).

Nicola Di Trani and Alessandro Grattoni are with the Department of Nanomedicine, Houston Methodist Research Institute, Houston, TX 77005 USA (e-mail: nditrani@houstonmethodist.org; agrattoni@houstonmethodist.org).

Digital Object Identifier 10.1109/JSEN.2023.3270521

also improving the efficacy and safety [5]. This is a critical goal as it will allow for the devices to be more easily accepted by patients and increase their willingness to use them. Furthermore, the ultimate goal is to include connectivity in these devices, which will allow to exchange information and personalize therapy [6], [7], thus improving their overall effectiveness. Primary batteries are one of the most common power sources used in AIMDs. They are widely used due to their ability to provide a stable and reliable power source for years; however, one of their major drawbacks is their large size. They take up a significant amount of space within the device, which can limit its overall design and functionality. On the other hand, secondary batteries, such as lithium-ion, can be used with a smaller size and capacity than primary cells: they will have a shorter life but they can be recharged periodically. Wireless power transfer (WPT) systems allow power to be delivered without the use of transcutaneous cables [8]. In the literature, different WPT methods such as inductive, near-field resonant inductive coupling (NRIC), near-resonant capacitive coupling (NCC), solar, and radio frequency are presented [1], [9], [10], [11]. NRIC devices enable the transmission of power ranging from tens to hundreds of milliwatts, which is compatible with secondary battery charging. Having an operational range in the order of the thickness of the skin, they are compatible with the power requirements and, in general, with the application scenario of small AIMDs. Indeed, this established technology has already powered a few commercial AIMDs [12]. As a result, it can be integrated into experimental subcutaneous implants that use receiving coils with a diameter of less than 2 cm to recharge secondary batteries. Overheating is a common problem in WPT systems, particularly in NRIC systems: according to European Standard EN45502-1 [13], an implanted device's temperature must not rise more than 2 °C over body temperature. The overheating is mainly due to the poor power transmission efficiency (PTE) and the low coil quality factor. Several factors, such as load variation, misalignment of the coils, and the distance between the coils, influence the PTE [10], [14]. Poor PTE means that more power is lost as heat, which can cause the system to overheat.

This article presents the design of an NRIC WPT system based on commercial off-the-shelf (COTS) components. The system is designed for charging secondary batteries and powering the nanochannel delivery system (nDS), a remotely controlled implantable platform for tunable drug delivery that features Bluetooth low-energy (BLE) connectivity [7], [15]. The integration of a rechargeable battery combined with a WPT system would enable the use of nDS in a preclinical setting targeting chronic experiments. Such a setting typically involves animal models and is focused on safety and efficacy/efficiency, thereby paving the way for long-term in vivo studies. In particular, the overall device size must not increase significantly, while recharge must occur safely, reliably, in short time, and respecting the regulations in term of biocompatibility, especially on overheating. The power transfer system under consideration must be designed to accommodate both near-static (long-term, slow, rare) and dynamic misalignments (short-term, quite fast, frequent, due to the animal's movement), to ensure an optimal power transfer for device charging. Indeed, the physical distance/alignment between the transmitting and receiving coils, as well as the tissues in between, may greatly affect the resulting electrical characteristics of the inductive link and can only be adjusted at implantation time. Therefore, a greater degree of robustness has to be accounted for at the design stage. The focus of this work is to investigate, given the mentioned requirements and constraints, the tradeoffs among coil miniaturization, overall system electrical performance, and coil temperature, all of which impact on the overall engineering of the final device and its suitability for different biomedical application scenarios. To improve the efficiency, robustness, and reliability of the wireless powering and charging system, we introduce a closed-loop control system leveraging the already available BLE link, with the ultimate goal of reducing dissipation and minimizing overheating. This article extends our previous work presented in [16] as a proof-of-concept with preliminary measurements. Here, we discuss in depth the behavior of the closed-loop WPT system using four different coils to effectively explore the pros and cons of different designs, with the crucial tradeoff between physical size and reliability across different and nonoptimal operating conditions. To further stress the robustness of the different solutions, we extended the range of the critical test conditions as well.

Section II presents and describes the nDS device and the WPT material. Section III presents the proposed closed-loop system and gives a description of the tests performed to validate it. Section IV describes the results, discussed in section V. Section VI presents the concluding remarks.

II. Materials

A. nDS System

The nDS is an AIMD for controlled drug administration, intended for the treatment of chronic pathologies [7], [15], [17]. It is based on a silicon nanofluidic membrane that modulates its permeability to the drug through the application of an electric potential, exploiting the electrochemical interaction between the drug molecules and the charged walls of the nanochannels. The nDS membrane allows for sustained systemic release of therapeutic agents, achieving a zero-order release kinetics that can be tuned to keep the plasma concentration of the drug in its therapeutic window, avoiding inefficacy and toxic effects [7]. Unlike commercial drug delivery devices, based on mechanical pumping and therefore bulky and power wasting, nDS would allow to extend controlled treatment to categories of patients that currently rely on traditional administration, with the advantage of improved medication adherence and reduced healthcare costs [18]. The current version of the device is shown in Fig. 1.

The printed circuit board (PCB) is sized 20 × 12 mm and includes a low-power wireless microcontroller unit (MCU), a digital temperature sensor for monitoring the surrounding environment, a membrane voltage management circuit based on a digital-to-analog converter (DAC), and a 2.4-GHz antenna. The MCU allows to remotely control the device using the BLE protocol. Membrane voltage can be set in a range between −3 and 3 V, which allows to efficiently tune drug release as previously demonstrated [7], [15], [17]. Temperature and battery level data are periodically monitored.

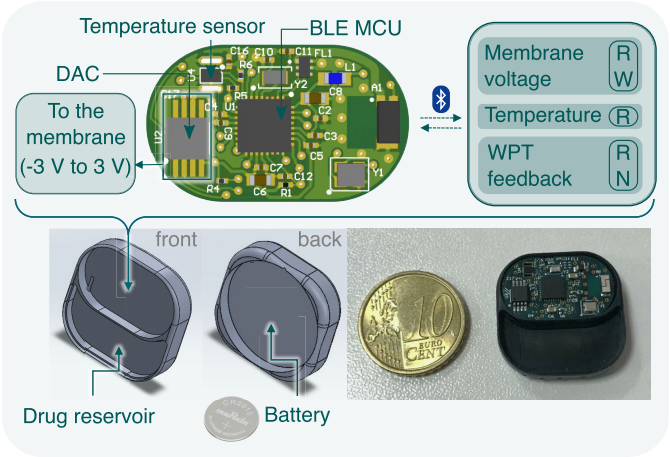

Fig. 1. nDS drug delivery device. The system is composed of a drug reservoir, closed by a biocompatible cap embedding the nanofluidic membrane (not represented), and a PCB powered by a battery. The PCB includes a BLE MCU, a temperature sensor, and the DAC for membrane control. BLE connectivity allows to read/write membrane voltage, read internal temperature, and read/notify the feedback for WPT.

Power consumption is kept low, thanks to system-level low-power techniques, other than the choice of integrating low-power components. In addition, the MCU firmware has been developed to minimize the power consumption by reducing as much as possible the radio-on and active-mode time. While settings like membrane voltage and reading intervals can only be changed during a BLE connection, read-only information is available in the advertising data. Thanks to these design choices, the devices proved 21 days of in vivo full operation with a 90-mAh battery (CR2016) [7]. The integration of power transmission control within the BLE services of this device allows to close the loop with zero impact on the device size and power consumption, and it allows, in this specific application, to bypass the need for data modulation on top of the inductive power link.

B. NRIC WPT System

The WPT system consists of an external transmitter and an internal receiver to be integrated into the implantable drug delivery system. The receiver is the most critical component, as it must comply with the constraints imposed by implantable devices. Therefore, choosing the smallest footprint IC that dissipates the most negligible power is necessary to not overheat the surrounding tissues. The LTC4124 [19] is a complete wireless power receiver with an integrated lithium battery charging system, occupying only a 4-mm^2 area and requiring only two external passive components compared with similar solutions. The other critical component of the receiver is the coil; different coils were considered and tested for this study, all summarized in Table I. The dimensions range between 6 and 19 mm in diameter, with the objective of identifying the most suited one for the intended application. Physical and biomedical constraints should be taken into account for the choice, given the nDS system physical and electrical requirements. The first two coils were chosen to be more compact in size, aiming to minimize the impact of the WPT system on the volume or, broadly speaking, the physical structure of the device. On the other hand, the other two coils were chosen larger for their reported electrical characteristics, possibly leading to a more efficient and reliable WPT.

TABLE I
RX COILS USED FOR THE TESTS. Q MEASURED WITH AGILET 4294A IMPEDANCE ANALYZER

Diameter (mm)	Thickness (mm)	Inductance (µH)	Q @200 kHz	Q measured @200 kHz
6[a]	3.3	8	N/A	15.45
12[b]	0.34	8.32	N/A	10.35
17[c]	0.82	12.6	25	27.99
19[d]	0.8	26	28	30.59

[a]Sunlord, MQQRC060630S8R0
[b]TDK, WR121210-27M8-ID
[c]Wurth Electronic, 760308101220
[d]Wurth Electronic, 760308101214

The LTC4125 [20] is an autoresonant wireless power transmitter compatible with the receiver. There are four possible types of resonant coupling: SS, SP, PS, and PP [21]. The first letter refers to the compensation in the TX (series or parallel), while the second letter denotes the resonant type in the receiver. SS and SP typologies deliver the same amount of power, but the first typology better works with high currents and low voltages, while the second one, vice versa, with high voltages and low currents. Choosing the SP typology improves the efficiency of the rectifier in the receiver when it operates at high voltage and is therefore the most suitable for implantable devices [21]. The LC tank of the TX consists of the coil and two parallel capacitors in series. The coil (Wurth Electronic, 760308101104) has an inductance of 6.8 µH and a diameter of 20.8 mm. The quality factor measured using the Agilent 4294A impedance analyzer is 57.1 (60.9 from the datasheet). The NRIC WPT system is tuned to a resonance frequency of 200 kHz.

III. METHODS

A. Closed-Loop Control

The LTC4125 IC plays a key role in optimizing WPT. We tested two power transmission approaches, one based on the integrated load-sensing system and the other on an effective closed-loop control system. In the first case, the LTC4125 executes a stepwise linear ramp of transmitted power at regular intervals to detect the presence or absence of a valid receiver. By measuring the magnitude of the LC tank voltage at each step, it can identify the optimal power transfer when a substantial change in peak tank voltage from one step to the next exceeds the hardware-set threshold. However, as indicated in the results section, the load-sensing control system results may be inconsistent and unreliable in different coil spatial conditions. Therefore, we introduced an effective closed-loop control system, external to the LTC4125, disabling the integrated load-sensing control. The goal of this system is to dynamically optimize the power transmission under different load conditions, which can vary depending on the spatial arrangement of the TX and RX. The closed-loop

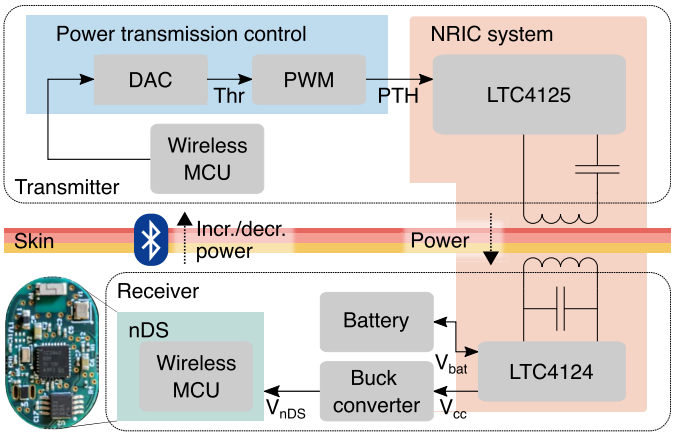

Fig. 2. Overview of the closed-loop NRIC WPT system used to test secondary battery charging and power nDS.

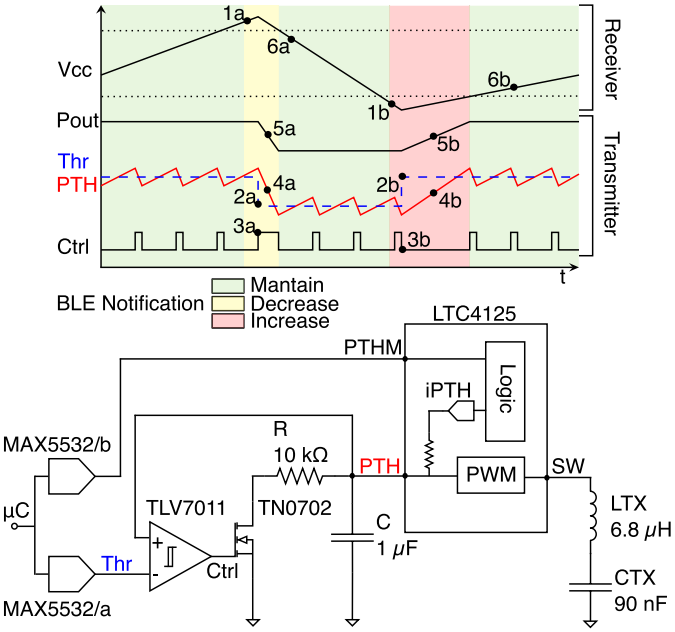

Fig. 3. Representation of the control system's operation when V_{CC} RX voltage increases/decreases (a/b): (1a/b) measurement of V_{CC} RX voltage and BLE notification; (2a/b) change in Thr value; (3a/b) control activation; (4a/b) PTH voltage variation; (5a/b) power transmission variation; (6a/b) V_{CC} voltage returns within the range (top). The simplified electrical circuit schematic of the TX control system (bottom).

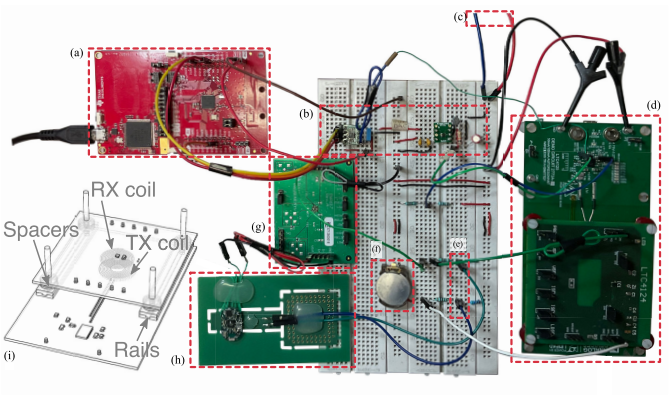

Fig. 4. Test bench setup for the recharge experiments, with main blocks highlighted: (a) TX MCU; (b) control system; (c) TX power supply; (d) coil and ICs support; (e) nDS ADC input for V_{CC} and V_{BAT}; (f) LIR2025 battery; (g) buck converter; (h) modified nDS PCB fixed on a support; and (i) detailed view of the coil and ICs support. The rails and the spacers were used for testing coil separation and misalignments. Power supply and measurement instrumentation are not shown for simplicity.

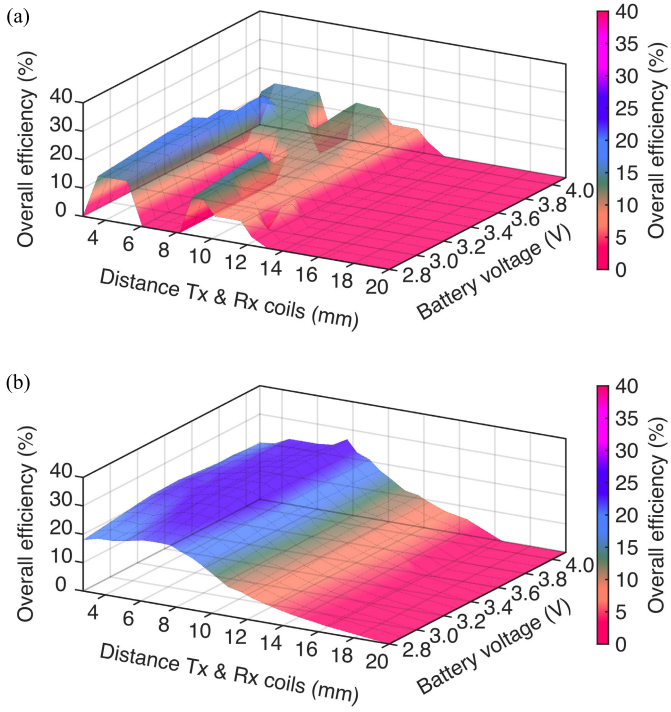

Fig. 5. Comparison of (a) load-sensing and (b) closed-loop NRIC WPT system efficiency. The test is conducted with 17-mm coil. In (a), 0% efficiency denotes that TX is unable to find the RX and consequently the power is not transmitted. Test conducted in air, charging current 10 mm, coil distance 2–20 mm, and simulated battery.

control shown in Fig. 2, split between TX and RX each with an MCU connected via BLE, is therefore used to enhance the performance of the WPT system in real-time. The control algorithm and hardware are designed as follows.

1) Algorithm: In the first phase of recharge, the RX MCU monitors the condition as follows:

$$V_{CC} > 3.6 \text{ V} \tag{1}$$

where V_{CC} is the rectified voltage on the receiver. This condition is fundamental to guarantee the correct working of the receiver. Unless this condition is satisfied, the MCU will request the transmitter to increase the transmission of power. Once the first condition is met, the RX MCU periodically checks condition as follows:

$$\begin{cases} V_{CC} - V_{BAT} < 300 \text{ mV}, & \text{Thr} \uparrow \\ 300 \text{ mV} \leq V_{CC} - V_{BAT} \leq 700 \text{ mV}, & \text{Thr} = \\ V_{CC} - V_{BAT} > 700 \text{ mV}, & \text{Thr} \downarrow \end{cases} \tag{2}$$

where V_{BAT} is the battery voltage. This condition is necessary to ensure proper battery charging, keeping V_{CC} voltage higher than the battery voltage. According to condition (2), the RX MCU sends a notification via BLE whether to maintain,

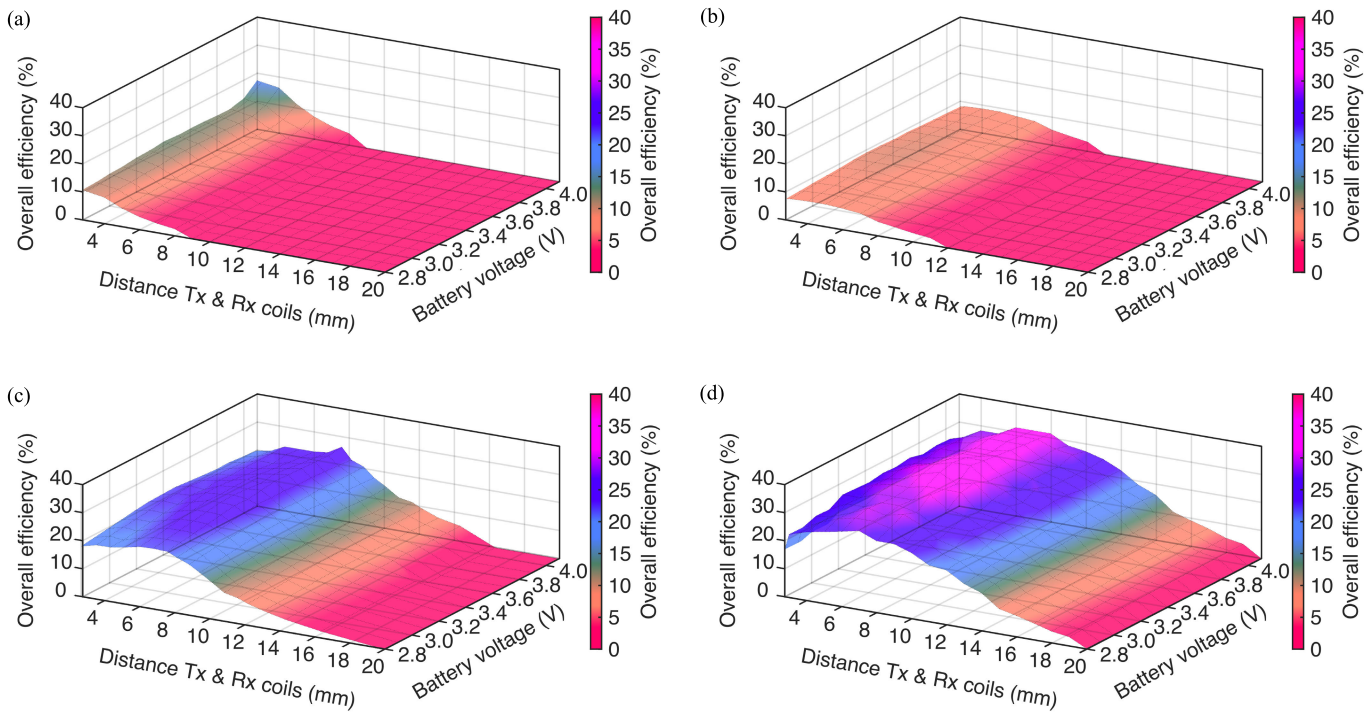

Fig. 6. NRIC WPT closed-loop system efficiency comparison using four different coils on the receiver: (a) coil 6 mm; (b) coil 12 mm; (c) coil 17 mm; and (d) coil 19 mm. Test conducted in air, charging current 10 mA, coil distance 2–20 mm, and simulated battery.

decrease, or increase the transmitted power. This whole task (conditions check and notification) is executed by the receiver every 2 s.

2) Hardware: The simplified electrical circuit schematic of the TX control system and a representation of closed-loop control are illustrated in Fig. 3.

The TX MCU increases, decreases, or maintains the LTV7011 comparator threshold (Thr) by a step size of 2.5 mV, according to the notification received via BLE. The capacitor is connected to the PTH pin of the LTC4125, and it is also feed back to the input of the comparator. The value of PTH is related to the power transmission; in fact, it adjusts the duty cycle of the square wave on the TX LC tank. The proposed NRIC WPT closed-loop system operates by charging and discharging the capacitor connected to the PTH pin [22]. The PTHM pin drives the charging process. The voltage on the PTHM defines the integrated DAC output (iPTH) (3) with an internal pull-up that continuously charges the capacitor [20]

$$\text{iPTH} = \frac{0.576}{0.24} \cdot \frac{\text{PTHM}}{V_{\text{DD}}}. \tag{3}$$

If the voltage on the PTH exceeds the set threshold, the comparator output switches to logic high, discharging the capacitor. When the transmitted power is to be kept stable, PTH oscillates around the threshold. The iPTH value also defines the maximum transmissible power. To prevent the threshold set by the MCU from exceeding iPTH, the MCU updates the PTHM value each time the threshold is changed as follows:

$$\text{PTHM} = 2 \cdot \text{Thr} + 200 \text{ mV}. \tag{4}$$

The LTC4125 maintains, however, its security mechanisms, specifically, the feature of disconnecting when the temperature on the coil exceeds 42 °C.

B. System Efficiency Characterization

Several factors impact the operation of an NRIC WPT system and, thus, energy transfer efficiency. One key factor is the distance between the transmitter and the receiver, which impacts the received power and the system's efficiency. In addition, the orientation, shape, size, and obstacles between the transmitter and the receiver can impact the performance of the NRIC WPT system. It is crucial to consider all these factors to achieve maximum energy transfer. We characterized the NRIC WPT closed-loop versus load-sensing control by varying the distance between the TX and RX coils and varying the load (battery voltage). The distances tested ranged from 2 to 20 mm with a step size of 1 ± 0.5 mm. We used a simulated battery by connecting a power supply to a 20-Ω resistor connected to the battery pin of the RX system. We used the same test bench to compare the closed-loop system with different receiver coils reported in Table I. We evaluated the robustness of the NRIC WPT system by investigating the effects of lateral misalignments ranging from 0 to 8 mm with increments of 1 mm and angular misalignments ranging from 0° to 12° with increments of 2°. We performed the experiments with a fixed coil spacing of 6.5 ± 0.5 mm. Considering that the device is intended for subcutaneous implantation, a test was performed using animal tissue (chicken breast) interposed between the coils [23], [24]. For each test, V_{BAT} is varied from 2.8 to 4.1 V with a step size of 0.1 V. This allowed to test

the efficiency for all the voltages in the constant current (CC) phase.

C. Battery Charging Tests

We performed charging tests using a coin battery LIR2025 with a capacity of 25 mAh and a charging current of 10 mA. The battery has a size and capacity compatible with the requirements of nDS. Fig. 4 depicts the experimental setup for the recharge tests, with emphasis on the main parts of the system, to showcase the relative positioning of circuit components. We conducted the tests with two different coil distances, 2.5 and 6.5 mm, and tested 12-, 17-, and 19-mm RX coils. On the transmitter, to verify the correct performance of the control algorithm, we monitored the PTH voltage and the temperature of the TX coil in real-time using NTC (Murata, FTN55XH103FD4B). At the same time, on the receiver, we measured the battery voltage (V_{BAT}), V_{CC}, the charging current (I_{BAT}), and the temperature of the RX coil using NTC (Semitec, 103JT-025). The overall efficiency (5) is calculated as follows:

$$\eta = \eta_{TX} \cdot \eta_{link} \cdot \eta_{RX} = (P_{BAT} + P_{nDS}) / P_{TX} \quad (5)$$

where P_{BAT} is the power required by the battery given by $V_{BAT} \cdot I_{BAT}$, P_{nDS} is the power required by nDS, powered at 3 V through a buck converter and an average current of 2 mA with the BLE connection active, and P_{TX} is the power supply of the transmitter. These tests aim to correlate recharge efficiency with coil temperature, focusing on the RX coil.

IV. Results

A. Closed-Loop Efficiency Charaterization

1) Load Sensing Versus Closed Loop: In Fig. 5, we report the results on transmission efficiency, tested on 17-mm coil, in the case of load-sensing control recharge and controlled recharge with closed loop. The load-sensing control in Fig. 5(a) has inconsistent (and unreliable) performance, resulting in no received power (0% efficiency) when the TX cannot detect the receiver. However, closed-loop control in Fig. 5(b) ensures successful and reliable power transfer, with no faults on the TX side. The efficiency of the system increases as the battery voltage increases and is highest for distances that match the thickness of skin. This outcome confirmed the hypothesis of the closed-loop as a possible solution to the reliability and continuity issues in power transfer and has prompted us to further examine the utilization of various coils to address the requirements of biocompatibility and miniaturization.

2) Voltage–Distance–Efficiency: The results of the coil characterization with respect to distance are reported in Fig. 6. In the tests on distance with the 6-mm coil [Fig. 6(a)], we were able to achieve a maximum distance of 9 mm before experiencing issues such as high power levels and consequent overheating of the transmitter, leading to the interruption of the power transmission. The peak efficiency is around 13% at 2 mm. With the 12-mm coil [Fig. 6(b)], we were able to reach a maximum distance of 11 mm before encountering similar problems. The peak efficiency is approximately 9% at 5 mm.

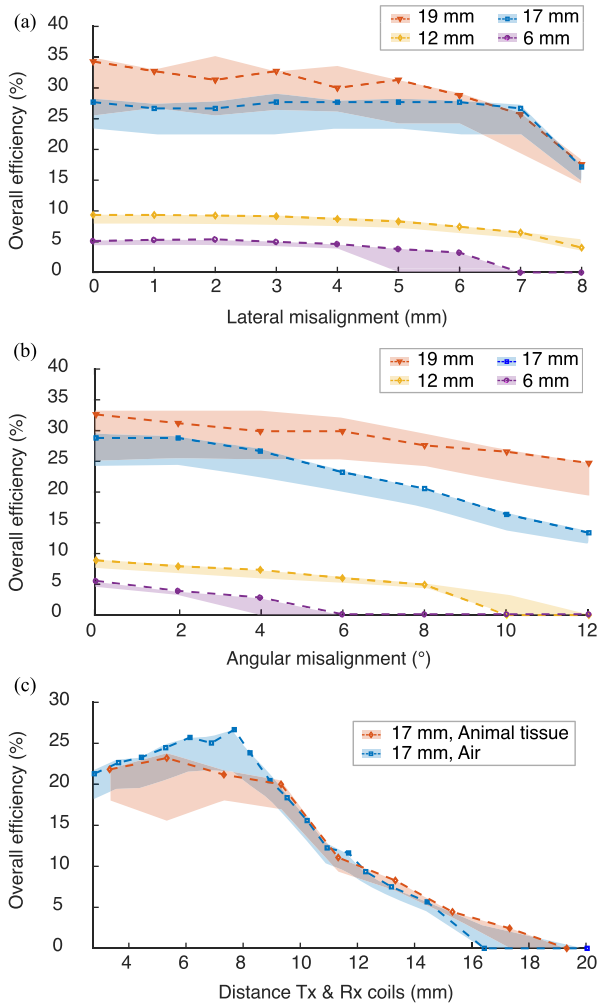

Fig. 7. Comparison of the overall efficiency of the NRIC WPT system under nonoptimal coupling conditions. (a) Lateral misalignment up to 8 mm, four coils tested. (b) Angular misalignment up to 12°, four coils tested. (c) Animal tissue (chicken breast) between coils, 17-mm coil tested. Dashed lines indicate efficiency measured with a simulated battery at 3.6 V. The bands indicate the change in efficiency with varying simulated battery loads from 2.8 to 4.1 V.

Although the 12-mm coil shows lower efficiencies than the 6-mm one, its performance is more consistent on distance. The 17- and 19-mm coils reach a maximum distance of 14 and 19 mm, respectively, before facing the same challenges [Fig. 6(c)–(d)]. The former shows a peak efficiency of 26% and the latter of 35%, both at 7 mm. Taking into account factors such as skin thickness, encapsulation, future transmitter housing, and PCB thickness, we chose a distance of 6.5 ± 0.5 mm as a common performance metric for the system. The efficiencies reported at that distance are 5%, 8.5%, 25.7%, and 31% for 6-, 12-, 17-, and 19-mm coils, respectively.

3) Misalignments: The test results for misalignment at 6.5 mm distance are shown in Fig. 7(a)–(b). Lateral misalignments are plotted in (a) and angular misalignments in (b). For the 6-mm coil, there is a relatively constant efficiency of 5% until 5 mm lateral misplacement, at which point the system begins to shut down due to overheating of the TX. On angular misalignment, efficiency begins to decrease significantly at 2° and the system shuts down at 4°. For the 12-mm coil, the efficiency is fairly consistent at 8% until 6 mm, and

TABLE II
CLOSED-LOOP SYSTEM PERFORMANCE DURING LIR2025 CHARGING TESTS AT 10 mA, MEASURED AT DIFFERENT DISTANCES *d* BETWEEN THE TX AND THE RX

d (mm)	Coil (mm)	Interposed medium	P_{TX} max. (mW)	P_{Load}** max. (mW)	η_{AVG} (%)	η_{MAX} (%)	V_{THR} max. (mV)	ΔT_{TX} max. (°C)	ΔT_{RX} max. (°C)
2.5	12	Animal tissue	604	51	6.6	9.5	571	14.7	18.7
2.5	12	0.9% Saline	505	46	6.6	9.7	523	5.3	9.3
2.5	12	Air	704	52	5.8	8.1	599	16.3	36.1
2.5	17*	Air	250	64.9	23.9	26.3	279	2.5	2.1
2.5	19	Air	220	52	21.1	24.3	292	3.5	4.9
6.5	12	Air	604	52	7.6	9.5	534	9.5	21.2
6.5	17*	Air	210	65.4	26.0	31.3	271	2.1	1.4
6.5	19	Air	180	56	26.3	32.3	251	1.4	1.7

* Results reported from [16]. ΔT_{RX} measured with thermal camera.
** P_{Load} is obtained by the sum of the power required by the battery (P_{BAT}) and that required by nDS (P_{nDS}).

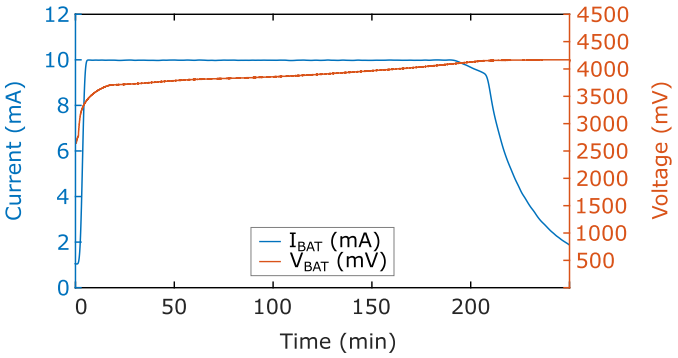

Fig. 8. Battery charging (pre-charge, CC, and CV phase) LIR2025 at 10 mm with the closed-loop system. Coil distance of 6.5 mm. RX coil 17 mm.

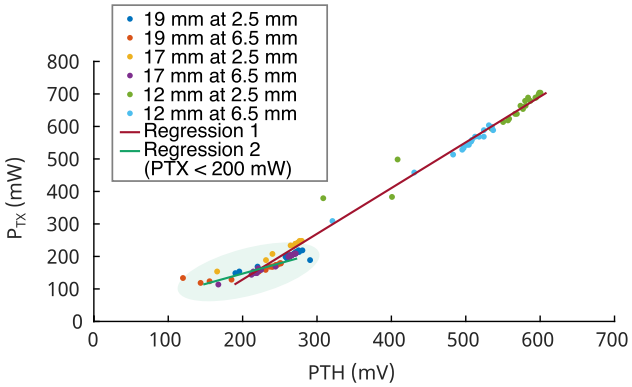

Fig. 9. Closed-loop PTH compared with P_{TX}. Data are collected during recharges of the LIR2025 battery using 12-, 17-, and 19-mm coils and TX and RX spacings from 2.5 to 6.5 mm. To show the correlation between PTH and P_{TX}, two regression lines are traced: the first one (Regression 1) is obtained using all the points in the chart; the second one (Regression 2) considering points with P_{TX} below 200 mW.

the system does not shut down within the analyzed range. Tests on angles show that efficiency is relatively constant at 8% until 4°, then lowers, with a drop to zero at 10°. The 17-mm coil maintains a practically constant efficiency of around 27%, and it begins to slightly decrease at 8 mm. On angular misalignments, the coil maintains a practically constant efficiency up to 4° of around 27%, and it begins to decrease significantly at 10° where efficiencies lower than 15% are observed. The 19-mm coil has a relatively constant efficiency of 30% until 6 mm of lateral displacement, and the system does not shut down in the analyzed range, maintaining an efficiency of 17% at 8 mm. Right above that distance, although there is a significant reduction in efficiency, it is very unlikely to have an abrupt drop in efficiency causing an unexpected shut down. The results for angular misalignment show a relatively constant efficiency of 30% until 10°. Again, no shut down was observed within 12°, while still maintaining an efficiency of 23%.

4) Biological Tissue: In Fig. 7(c), we report the results obtained using biological tissue (chicken breast) as a medium interposed between the TX and RX coils. We used the 17-mm coil, and the chicken breast as a phantom. A slight decrease in efficiency is observed; however, we may not consider it significant.

B. Battery Charging Performance

1) Charging Process: The battery recharge tests were conducted using an LIR2025 battery, which was selected as the optimal balance between capacity, charging time, duration between recharges, and physical dimensions. A three-stage process can be identified in the charging procedure, comprising pre-charge, CC, and constant voltage (CV) phases (Fig. 8). The pre-charge phase, in which the current supplied to the battery is below 10 mA, prevents damage to excessively discharged batteries. Once the voltage surpasses 2.8 V, the current gradually increases from 1 to 10 mA. The CC phase starts once the current reaches this final value, in which the current is maintained constant, and the battery voltage increases, reaching 4.2 V. At this point, the current begins to decrease and the charging process can be terminated. With this method, complete and safe charging of the LIR2025 battery is achieved within 250 min from the beginning of the recharge process. Fig. 9 shows the relationship between PTH and P_{TX}, illustrating how the closed-loop system adjusts the transmitted power according to different loads.

TABLE III
COMPARISON OF COILS WITH RESPECT TO THE DEVICE REQUIREMENTS

Coil (mm)	Size	Robustness	Efficiency	Δ T
6	++	-	-	/
12	++	+	-	-
17	+	++	+	++
19	+	++	++	++

Symbols used and meaning: (-) bad, (+) good, (++) very good

The results obtained from the continuous monitoring of recharge tests, which were carried out using the nDS connection, are presented in Table II. For both the coil distances of

TABLE IV
COMPARISON WITH SIMILAR NRIC SOLUTIONS FOR AIMDS, ORDERED BY DECREASING TX POWER

Reference	P_{TX} *(W)*	*freq. (kHz)*	$\varnothing_{TX}$ (mm)	$\varnothing_{RX}$ (mm)	d (mm)	η *(%)*	*Application*
[28]	48	50	N/A	N/A	10	72	Artificial heart
	12	50	N/A	N/A	10	62	
[29]	10–60	120	N/A	N/A	10	66–78	Artificial heart
[30]	1	206	74	71.2	11.6	12.5	General
[31]	0.810	125	22	11	10	29.9	Neural
This work	0.210	200	21	19	6.5	32.3	Drug delivery
[32]	0.137	700	60	20	30	36	Orthopaedic

2.5 and 6.5 mm we report the interposed medium, the power required by the transmitter and the receiver, the average and maximum efficiency, the maximum value of PTH, and the maximum temperature variation on the TX and RX coils.

V. DISCUSSION

The coil tests allow to identify the potential of their future use in battery charging in the experimental conditions of an in vivo recharge. For example, while the 6-mm coil performed better in terms of maximum efficiency and had smaller dimensions compared with the 12-mm coil, it did not move to the recharge test phase due to its inability to ensure robustness under possible in vivo conditions, where movements of the animal inevitably lead to misalignments. This is a proof that efficiency under a specific condition alone is not a sufficient metric for determining the quality of the system in applications where strong robustness and reliability are required under varying conditions. In terms of performance, the 19-mm coil proves to be the best, both considering efficiency and its ability to withstand nonoptimal operating conditions, showing the best performance for both angular and lateral misalignments. The 6-mm coil, on the other hand, is the worst performer with a low efficiency (5%) on the useful distance and it is too susceptible to changes in coupling conditions, despite a peak of 13% at 2-mm distance. The 12-mm coil, still advantageous to fulfill miniaturization requirements, is not discarded because of its higher efficiency on the useful distance (8.5%) and more robust to misalignments than the 6-mm one. The test results show that increasing the diameter sensitively improves the efficiency of the system. At the same time, the efficiency of the system is maximized at a specific distance; by reducing the gap, the efficiency will not improve, despite the corresponding increase in the coupling factor. Indeed, here (see 5) we are including the term η_{TX} related to the TX as well, and this can negatively impact the overall efficiency.

The results of the battery charging tests demonstrate the smooth and consistent nature of the charging process, with no instances of malfunction or interruption, in accordance with the expected CC-CV charging profile [25] as shown in Fig. 8. At the same time, nDS shows complete and correct functionality, maintaining the BLE link with the transmitter, allowing to access the service, and keeping notification of threshold data active. As expected, in comparison to the 19-mm coil, the 12-mm coil requires a higher transmitted power to charge the battery, as evidenced by evaluating PTH, which is nearly double that required by 19 mm. The increase in power also results in an increase in power dissipated by the coils, leading to an unacceptable increase in temperature for both the transmitter and the receiver, exceeding 60°C in air. The assessment of thermal performance in the WPT system is a crucial aspect in biomedical applications, which is often overlooked and challenging to accomplish [26]. While not causing a significant performance decrease, tissue interposition has been observed to assist in regulating the temperature increase through its water content and its thermal capacitance. The results obtained with the interposition of saline solution further prove that media with a high content of water play a vital role in regulating the temperature increase. The mitigation effect of tissue on overheating is therefore expected to be enhanced in environments characterized by blood perfusion [27]. The presented system demonstrates highly favorable outcomes, as evidenced by the data presented in Table II; the 17-mm coil is the smallest one that guarantees proper charging without overheating, obtaining the best performance together with the 19-mm one, as summarized in Table III.

To better understand how the control algorithm effectively adapts the transmitted power, in Fig. 9 a set of operating points during a charging process are reported. They are grouped by RX coil size and TX/RX distance, thereby each set represents a different setup and/or operating condition, or, from an electrical perspective, different load conditions. Given a set of points, their dispersion shows, broadly speaking, how much the closed loop has to adapt in real-time the transmitted power P_{TX} by setting PTH; in particular the dispersion at low powers (below 200 mW, with PTH varying from 100 to 250 mV) is more pronounced than at higher power levels, where presumably the TX IC has the optimal working point [20]. By looking at the possible relations between these two quantities (highlighted by regression lines in Fig. 9), it is easy to spot different sensitivities at different power levels, further confirming the need for an adaptive control for an efficient and reliable WPT with changing (and not precisely predictable) load conditions.

Table IV shows comparison of the performance of our work with other NRIC WPT systems that have been reported in the literature for biomedical applications. Considering efficiency as the most widespread performance metric, our system is comparable to other solutions with similar operating frequency and levels of transmitted power. Sensitively higher efficiencies are only found for transmitted powers of the order of tens of watts. The decrease in the PTE resulting from lower levels of transmitted power is systematic in NRIC systems, found also in higher power applications [28], as well as the reduction in performance in response to load variations with respect to the optimal conditions for which the WPT was designed [32]. This further remarks the need for an approach that is robust with respect to the variation in configuration when a static, fixed

setup cannot be guaranteed, as in case of long-term chronic studies with implantable devices.

VI. Conclusion

In this study, a closed-loop NRIC WPT system composed of commercially available components was developed and tested in conjunction with an experimental AIMD for drug-delivery applications. The method used allows the advantageous use of COTS parts respecting thermal and geometrical constraints. The results of the experiments demonstrate the stability of power transfer, with minimal overheating and satisfactory efficiency with the coils of 17 and 19 mm. Table III summarizes the comparison of coils concerning the requirements of the system. The findings of this research are promising in the context of long-term implantation for chronic animal studies [17], [33]. The recharge capability of a 25-mAh battery allows for an estimated activity of the drug delivery system for a minimum of 5 days, proportionally to what is reported in [7] for the 90-mAh primary cell (CR2016). The selected battery is capable of up to 500 recharge cycles, yielding a projected chronic duration of greater than 6 years.

In future work, the integration of the WPT system into the nDS PCB will be developed, and therefore the whole device re-engineered from a system perspective. Furthermore, the battery's actual longevity will be evaluated through examination of a recharge and discharge process of the new nDS device.

References

[1] K. Agarwal, R. Jegadeesan, Y. Guo, and N. Thakor, "Wireless power transfer strategies for implantable bioelectronics," *IEEE Rev. Biomed. Eng.*, vol. 10, pp. 136–161, 2017.

[2] J. S. Ho, S. Kim, and A. S. Y. Poon, "Midfield wireless powering for implantable systems," *Proc. IEEE*, vol. 101, no. 6, pp. 1369–1378, Jun. 2013.

[3] F. P. Pons-Faudoa et al., "Preventive efficacy of a tenofovir alafenamide fumarate nanofluidic implant in SHIV-challenged nonhuman primates," *Adv. Therapeutics*, vol. 4, no. 3, 2021, Art. no. 2000163.

[4] F. P. Pons-Faudoa, A. Ballerini, J. Sakamoto, and A. Grattoni, "Advanced implantable drug delivery technologies: Transforming the clinical landscape of therapeutics for chronic diseases," *Biomed. Microdevices*, vol. 21, no. 2, p. 47, May 2019.

[5] J. S. Ho et al., "Wireless power transfer to deep-tissue microimplants," *Proc. Nat. Acad. Sci. USA*, vol. 111, no. 22, pp. 7974–7979, Apr. 2014.

[6] G. Bruno et al., "The active modulation of drug release by an ionic field effect transistor for an ultra-low power implantable nanofluidic system," *Nanoscale*, vol. 8, no. 44, pp. 18718–18725, 2016.

[7] N. Di Trani et al., "Remotely controlled nanofluidic implantable platform for tunable drug delivery," *Lab Chip*, vol. 19, no. 13, pp. 2192–2204, 2019.

[8] Y. Zhou, C. Liu, and Y. Huang, "Wireless power transfer for implanted medical application: A review," *Energies*, vol. 13, no. 11, p. 2837, Jun. 2020.

[9] G. L. Barbruni, P. M. Ros, D. Demarchi, S. Carrara, and D. Ghezzi, "Miniaturised wireless power transfer systems for neurostimulation: A review," *IEEE Trans. Biomed. Circuits Syst.*, vol. 14, no. 6, pp. 1160–1178, Dec. 2020.

[10] S. R. Khan, S. K. Pavuluri, G. Cummins, and M. P. Y. Desmulliez, "Wireless power transfer techniques for implantable medical devices: A review," *Sensors*, vol. 20, no. 12, p. 3487, Jun. 2020.

[11] A. N. Khan, Y.-O. Cha, H. Giddens, and Y. Hao, "Recent advances in organ specific wireless bioelectronic devices: Perspective on biotelemetry and power transfer using antenna systems," *Engineering*, vol. 11, pp. 27–41, Apr. 2022.

[12] M. Haerinia and R. Shadid, "Wireless power transfer approaches for medical implants: A review," *Signals*, vol. 1, no. 2, pp. 209–229, Dec. 2020.

[13] *Active Implantable Medical Devices—Part 1: General Requirements for Safety, Marking and Information to be Provided by the Manufacturer*, Standard 45502-1, 1997.

[14] H.-J. Kim, H. Hirayama, S. Kim, K. J. Han, R. Zhang, and J.-W. Choi, "Review of near-field wireless power and communication for biomedical applications," *IEEE Access*, vol. 5, pp. 21264–21285, 2017.

[15] A. Silvestri et al., "Silicon carbide-gated nanofluidic membrane for active control of electrokinetic ionic transport," *Membranes*, vol. 11, no. 7, p. 535, Jul. 2021.

[16] F. Del Bono, A. Bontempi, N. Di Trani, D. Demarchi, A. Grattoni, and P. M. Ros, "Wireless power transfer closed-loop control for low-power active implantable medical devices," in *Proc. IEEE Sensors*, Oct. 2022, pp. 1–4.

[17] N. Di Trani et al., "Electrostatically gated nanofluidic membrane for ultra-low power controlled drug delivery," *Lab Chip*, vol. 20, no. 9, pp. 1562–1576, 2020.

[18] J. C. Quarterman, S. M. Geary, and A. K. Salem, "Evolution of drug-eluting biomedical implants for sustained drug delivery," *Eur. J. Pharmaceutics Biopharmaceutics*, vol. 159, pp. 21–35, Feb. 2021.

[19] *100 mA Li-Ion Charger With Low Battery Disconnect, Analog Devices*, Standard LTC4124, 2019. [Online]. Available: https://www.analog.com/en/products/ltc4124.html

[20] *5W AutoResonant Wireless Power Transmitter, Analog Devices*, Standard LTC4125, 2015. [Online]. Available: https://www.analog.com/en/products/ltc4125.html

[21] R. Jegadeesan and Y. X. Guo, "Topology selection and efficiency improvement of inductive power links," *IEEE Trans. Antennas Propag.*, vol. 60, no. 10, pp. 4846–4854, Oct. 2012.

[22] W. Li, "Close the loop between wireless charger receiver and transmitter without digital controllers," Analog Devices, Wilmington, MA, USA, Tech. Rep. TA21874-1/20, 2020.

[23] R. K. Pokharel, A. Barakat, S. Alshhawy, K. Yoshitomi, and C. Sarris, "Wireless power transfer system rigid to tissue characteristics using metamaterial inspired geometry for biomedical implant applications," *Sci. Rep.*, vol. 11, no. 1, p. 5868, Mar. 2021, doi: 10.1038/s41598-021-84333-3.

[24] X. Jiang, F. Tahar, T. Miyamoto, A. Barakat, K. Yoshitomi, and R. K. Pokharel, "Efficient and compact dual-band wireless power transfer system through biological tissues using dual-reference DGS resonators," in *IEEE MTT-S Int. Microw. Symp. Dig.*, Jun. 2021, pp. 54–57.

[25] E. Ayoub and N. Karami, "Review on the charging techniques of a Li-ion battery," in *Proc. 3rd Int. Conf. Technological Adv. Electr., Electron. Comput. Eng. (TAEECE)*, Apr. 2015, pp. 50–55.

[26] I. Williams et al., "SenseBack—An implantable system for bidirectional neural interfacing," *IEEE Trans. Biomed. Circuits Syst.*, vol. 14, no. 5, pp. 1079–1087, Oct. 2020.

[27] K. Hynynen, D. Deyoung, M. Kundrat, and E. Moros, "The effect of blood perfusion rate on the temperature distributions induced by multiple, scanned and focused ultrasonic beams in dogs kidneys in vivo," *Int. J. Hyperthermia*, vol. 5, no. 4, pp. 485–497, Jan. 1989, doi: 10.3109/02656739909140473.

[28] A. Ghahary and B. H. Cho, "Design of transcutaneous energy transmission system using a series resonant converter," *IEEE Trans. Power Electron.*, vol. 7, no. 2, pp. 261–269, Apr. 1992.

[29] G. B. Joun and B. H. Cho, "An energy transmission system for an artificial heart using leakage inductance compensation of transcutaneous transformer," *IEEE Trans. Power Electron.*, vol. 13, no. 6, pp. 1013–1022, Nov. 1998.

[30] M. A. Adeeb, A. B. Islam, M. R. Haider, F. S. Tulip, M. N. Ericson, and S. K. Islam, "An inductive link-based wireless power transfer system for biomedical applications," *Act. Passive Electron. Compon.*, vol. 2012, pp. 1–11, Jan. 2012.

[31] M. Ghovanloo and S. Atluri, "A wide-band power-efficient inductive wireless link for implantable microelectronic devices using multiple carriers," *IEEE Trans. Circuits Syst. I, Reg. Papers*, vol. 54, no. 10, pp. 2211–2221, Oct. 2007.

[32] M. Catrysse, B. Hermans, and R. Puers, "An inductive power system with integrated bi-directional data-transmission," *Sens. Actuators A, Phys.*, vol. 115, nos. 2–3, pp. 221–229, Sep. 2004. [Online]. Available: https://www.sciencedirect.com/science/article/pii/S0924424704001335

[33] A. Grattoni et al., "Nanochannel systems for personalized therapy and laboratory diagnostics," *Current Pharmaceutical Biotechnol.*, vol. 11, no. 4, pp. 343–365, Jun. 2010.

Fabiana Del Bono (Graduate Student Member, IEEE) received the B.Sc. degree in biomedical engineering and the M.Sc. degree from Politecnico di Torino, Turin, Italy, in 2018 and 2020, respectively, and the M.Sc. degree from Politecnico di Milano, Milan, Italy, in 2021. She is currently pursuing the Ph.D. degree in electrical, electronics, and communications engineering with the MiNES (Micro and Nano Electronics Systems) Group, Politecnico di Torino.

Her main research interests include design of implantable medical devices, bioelectronics, and wireless power transfer and communication systems. Since 2021, she has been a member of the Executive Committee of the IEEE Student Branch, Politecnico di Torino, where she is currently serving as the Vice-Chair.

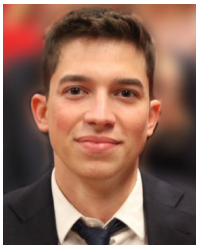

Andrea Bontempi (Graduate Student Member, IEEE) received the B.Sc. and M.Sc. degrees in biomedical engineering from Politecnico di Torino, Turin, Italy, in 2018 and 2021, respectively. He is currently pursuing the Ph.D. degree with the Department of Electronics and Telecommunication (DET), MiNES (Micro and Nano Electronic Systems) Research Group.

Since 2021, he has been the Treasurer of the IEEE Student Branch, Politecnico di Torino. His research focuses on electronic and microelectronic system applied to biomedical devices.

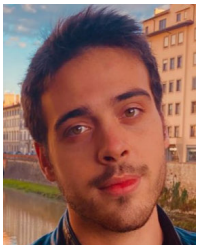

Andrea Dentis received the B.Sc. degree in biomedical engineering from Politecnico di Torino, Turin, Italy, in 2020. He is currently pursuing the master's degree in mechatronic engineering with Politecnico di Torino, and is carrying out his master's thesis at the MiNES (Micro and Nano Electronic Systems) Research Group. He has a great interest in electronics and robotics, especially in the biomedical environment.

Nicola Di Trani received the B.S. and M.S. degrees in biomedical engineering from Politecnico di Torino, Turin, Italy, in 2015 and 2017, respectively, and the Ph.D. degree in material science and engineering from the University of Chinese Academy of Sciences, Beijing, China, in 2021.

He is currently a Postdoctoral Fellow in the laboratory of Dr. Alessandro Grattoni at the Houston Methodist Research Institute, Houston, TX, USA. During his Ph.D. and postdoctoral, he has been working on the development of implantable devices for drug delivery. These devices are aimed at the treatment and/or management of a variety of chronic pathologies including hypertension, cancer, and HIV prophylaxis. He is an author and a coauthor of more than 20 peer-reviewed scientific publications in the field of drug delivery, nanofluidics, HIV PrEP, cancer and material science.

Danilo Demarchi (Senior Member, IEEE) received the engineering degree and the Ph.D. degree in electronics engineering from Politecnico di Torino, Turin, Italy, in 1991 and 1995, respectively.

From 2018 to 2021, he was a Visiting Professor at Tel Aviv University, Tel Aviv, Israel, and at the École Polytechnique Fédérale de Lausanne (EPFL), Lausanne, Switzerland, in 2019. He was a Visiting Scientist at the Massachusetts Institute of Technology (MIT), Boston, and Harvard Medical School, Boston, MA, USA, in 2018. He is a Full Professor at the Department of Electronics and Telecommunications, Politecnico di Torino. He is an author and a coauthor of five patents and more than 300 international scientific publications.

Prof. Demarchi is a member of IEEE Sensors Council and a member of the IEEE BioCAS Technical Committee. He is the Leader of the MiNES (Micro and Nano Electronic Systems) Laboratory at Politecnico di Torino, and an Associate Editor of IEEE SENSORS JOURNAL, IEEE OPEN JOURNAL OF ENGINEERING IN MEDICINE AND BIOLOGY, and *Springer Journal BioNanoScience*, the General Chair of IEEE BioCAS in 2017, and the Founder of the IEEE FoodCAS Workshop (Circuits and Systems for Better Quality Food).

Alessandro Grattoni received the M.S. degree in mechanical engineering and the Ph.D. degree in biomedical engineering from Politecnico di Torino, Turin, Italy, in 2005 and 2009, respectively.

In 2010, he completed a Postdoctoral training in nanotechnology in Dr. Mauro Ferrari's laboratory at the Brown Foundation Institute of Molecular Medicine, University of Texas Health Science Center, Houston, TX, USA. In 2010, he was appointed as an Assistant Professor at the Department of Nanomedicine, Houston Methodist Research Institute (HMRI), Houston. Currently, he is the Frank J. and Jean Raymond Centennial Chair, and the Chairman and a Professor at the Department of Nanomedicine, HMRI. His research activities are dedicated to the development and clinical translation of implantable technology platforms for controlled long-acting drug delivery and cell transplantation. Active areas of research include HIV pre-exposure prophylaxis (PrEP), metabolic syndrome, and intratumoral cancer immunoradiotherapy. In addition, his laboratory is actively studying electrokinetics in nanofluidics for modulating molecular transport to achieve a remotely controlled drug delivery platform for telemedicine. Further area of research is 3-D-manufactured microencapsulation devices for the transplantation of endocrine cells. The primary focus is the creation of a protected environment supporting cell transplantation, long-term viability, and function. Areas of applications include type 1 diabetes and hypogonadism among others. With the support for the ISS National Laboratory, he has established a Center for Space Nanomedicine at the Houston Methodist Research Institute, fully focused on leveraging the microgravity laboratory of the International Space Station, for the investigation of nanomedicine approaches for the benefit of patients on-Earth and for space exploration. He is the Founder and the Scientific Advisor for two spin-off companies, Semper Therapeutics and NanoGland, which are focused on the clinical translation of the technology platforms developed in his laboratory.

Paolo Motto Ros (Member, IEEE) received the M.Sc. and Ph.D. degrees in electronic engineering from Politecnico di Torino, Turin, Italy, in 2005 and 2009, respectively.

From 2009 to 2012, he was a Postdoctoral Researcher at Politecnico di Torino, a Senior (since 2014) Postdoctoral Researcher at Istituto Italiano di Tecnologia, Genoa, Italy, from 2012 to 2019, a Senior Postdoctoral Researcher, and an Adjunct Professor (since 2017) at Politecnico di Torino, from 2019 to 2022. He is an Assistant Professor at the Department of Electronics and Telecommunications, Politecnico di Torino. He is an author and a coauthor of more than 80 international scientific publications.

Dr. Motto Ros was a member of the organizing committee of IEEE ICECS in 2019, the FoodCAS Satellite Event at IEEE ISCAS in 2021, and IEEE CAFE in 2023, a review committee member of IEEE BioCAS in 2021 and 2022, a special session organizer at IEEE MeMeA in 2021, a program committee member of IEEE LASCAS in 2022, a Guest Editor of MDPI Sensors, and a Guest Associate Editor of *Frontiers in Neurorobotics*. He is an Associate Editor of IEEE TRANSACTIONS ON AGRIFOOD ELECTRONICS and IEEE TRANSACTIONS ON BIOMEDICAL CIRCUITS AND SYSTEMS.

Open Access funding provided by 'Politecnico di Torino' within the CRUI CARE Agreement